Characterization of a 90° waveguide bend using near-field scanning optical microscopy

Guangwei Yuan[a] and Kevin L. Lear[b]
Department of Electrical and Computer Engineering, Colorado State University, Fort Collins, Colorado 80523

Matthew D. Stephens and David S. Dandy
Department of Chemical and Biological Engineering, Colorado State University, Fort Collins, Colorado 80523

(Received 5 July 2005; accepted 9 September 2005; published online 1 November 2005)

Multiple modes are directly imaged in a silicon nitride waveguide bend using near-field scanning optical microscopy. Since the high order mode attenuates faster than the fundamental mode, a transient interference is observed. Local loss at the bend-to-straight waveguide interface is found and attributed to modal mismatch. The observations are in good agreement with modal calculations using conformal index transformation. © *2005 American Institute of Physics*.
[DOI: 10.1063/1.2126135]

Waveguide bends are frequently used in photonic integrated circuits and optical sensors. Several theoretical models have been used to investigate modes in waveguide bends.[1,2] Among them, the conformal index transformation method is regarded as a simple and effective method to solve for the mode profile. However, experimental observations have not previously been reported on the evolution of modes in waveguide bends.

To characterize a waveguide bend, near-field scanning optical microscopy (NSOM) is used to directly measure the evanescent field on the upper surface of the waveguide. The NSOM technique has been employed for straight waveguides, as well as curved waveguides, to characterize propagation loss, spatial mode profiles, and modal interference.[3–8] The NSOM instrument used is an α-NSOM system from WiTec that is able to simultaneously measure light intensity and surface height. The system has a lateral-scanning resolution of approximately 10 nm. It relies on a microfabricated hollow aluminum pyramidal tip to convert an evanescent wave to a propagating wave by locally frustrated total internal reflection.[9] A subwavelength size pinhole centered in the tip is initially aligned to maximize the signal received by a photomultiplication tube. Similar tips can also be found in generic atomic force microscopy systems, but without apertures. A reference laser beam is reflected from the tip cantilever to a segmented photodetector to determine the topography of the waveguide sample. Figure 1 illustrates a three-dimensional (3D) NSOM surface height plot of a waveguide bend.

The 90° waveguide bend studied here was fabricated using traditional sputtering, optical lithography, and etching processes. The 110-nm-thick rib waveguide core of index 1.8 is made of SiN_x and sits on a 2-μm-thick SiO_2 lower cladding of index 1.45 deposited on a Si wafer. A 4-μm-wide rib waveguide core was defined by partially dry etching the surrounding SiN_x layer in a CF_4/O_2 gas. Air serves as the upper cladding allowing NSOM measurements of the evanescent field above the core. The waveguide had a centerline bending radius of $R_c=400$ μm. Although this is a 3D waveguide structure, two-dimensional effective index conformal mapping is sufficient to determine the lateral mode profiles. Before mapping, the waveguide core region has an effective index of 1.468 surrounded by a region with an effective index of 1.45, as illustrated in Fig. 2. The inner radius of the core is $R_1=398$ μm and the outer radius is $R_2=402$ μm. The angle between the interface where the straight waveguide enters the bend and the position being studied is θ. The waveguide sample was facet polished and coupled with a visible, 654 nm, laser diode using single mode (4/125 μm diameter) fiber. NSOM measurements simultaneously yielded light intensity and topography images, allowing the lateral mode position in the waveguide to be determined. Figure 3 illustrates the intensity distribution in the bending waveguide segments centered at $\theta=20°$, 40°, 60°, and 80°, with dotted lines showing the measured topographic edge of the ridge. Each scanned area is 25 μm$\times$25 μm. Strong modal interference is observed at 20°, but diminishes further along the bend. Although the bent waveguide supports a fundamental mode ($m=0$) as well as a higher order mode ($m=1$), the latter attenuates much faster than the fundamental. At larger angles ($\theta=60°$ and 80°), modal profiles become smooth, as the fundamental mode dominates the beam profiles.

A conformal index transformation based on new coordinate parameters $u(r)=R_2\ln(r/R_2)$ and $n(u)=n(r)e^{u/R_2}$ were used to solve for the waveguide modes in the bend. As a

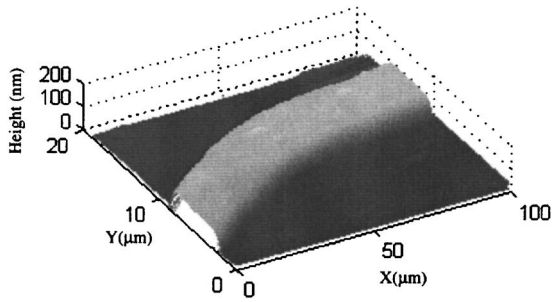

FIG. 1. (Color online) 3D NSOM surface height plot.

[a]Electronic mail: gwyuan@engr.colostate.edu
[b]Electronic mail: kllear@engr.colostate.edu

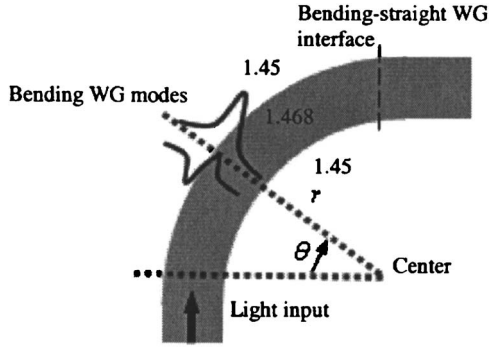

FIG. 2. Schematic diagram (not to scale) of a 90° waveguide bend connected to straight sections. The effective index of the waveguide core and cladding regions are 1.468 and 1.45. The waveguide bend supports two guided modes.

result, a tilted effective index profile is shown in Fig. 4(a) with arrows corresponding to the outer (I) and inner (II) core boundaries. The calculation found only two lateral TE modes ($m=0$ and 1) can be supported in this waveguide bend. Effective indexes for both modes are illustrated in Fig. 4(a) by two dashed lines, which are $\beta_0/k_0=1.461$ and $\beta_1/k_0=1.454$ where β_m is the propagation constant for the mth mode and k_0 is the free space wave vector. H-field profiles of the two modes in the waveguide bend are plotted in Fig. 4(b). Dashed lines indicate the waveguide core boundaries. These modes are similar in shape to those for the straight waveguide but are shifted off center toward the outer boundary.

The evolution of the transverse mode profiles is illustrated in Fig. 5. The measured values at different angles are shown as points, and theoretical fitting curves are shown as solid lines. The intensity profiles clearly show the presence of multimode interference which decays along the length of the bend. In particular, at 80° the mode profile is dominated by the fundamental mode. To extract the attenuation coefficients for the two modes, α_0 and α_1, in the presence of interference, the total magnetic field due to the interfering modes is expressed as $H(\theta,r)=A_0H_0(r)\exp(i\beta_0R_c\theta-\alpha_0R_c\theta)$ $+A_1H_1(r)\exp(i\beta_1R_c\theta+i\phi-\alpha_1R_c\theta)$, where $A_0=0.96$ and $A_1=3.4$ are the relative amplitudes of the two modes, $H_m(r)$ is the transverse field distribution of the mth mode, and $\phi=0.74\pi$ is the relative phase difference in the modes at the start of the bend. Relative amplitudes of these modes are obtained by fitting the measured NSOM intensity profiles. Similarly, by fitting the evolution of the profile as well as the combined intensity, it is estimated that the attenuation loss of the fundamental and the first order mode are 0.46 dB/90° and 15.1 dB/90°, respectively. The extracted coefficients produce transverse intensity profiles in good agreement with the NSOM measurements. Similar to the use of tightly coiled fibers to strip higher order modes, the greater than 14 dB difference in attenuation of the first higher order mode demonstrates that planar waveguide bends can be used as practical mode filters.

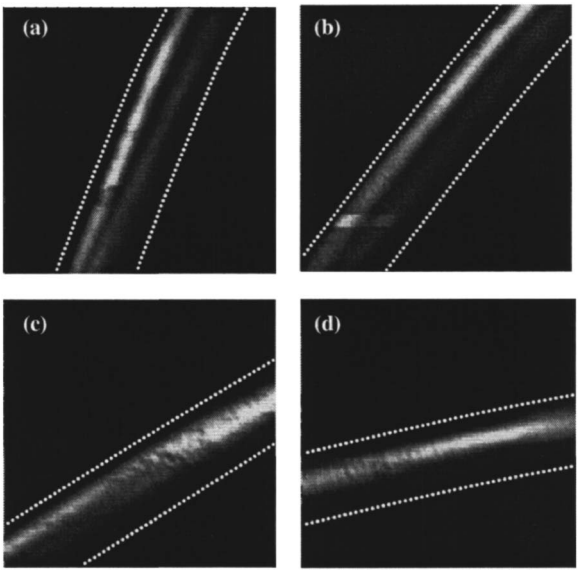

FIG. 3. NSOM images of optical intensity at (a) 20°, (b) 40°, (c) 60°, and (d) 80°, from the start of the waveguide bend. Dotted lines denote the waveguide core boundaries. As determined from simultaneous topographical scans.

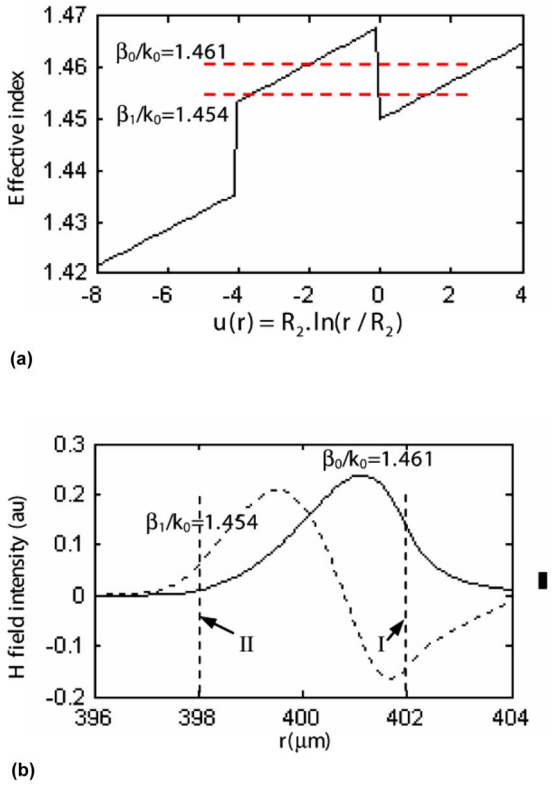

FIG. 4. (a) Effective refractive index profile in the waveguide bend. Dashed lines mark the effective indexes of the guided modes. (b) H-field profiles of the guided modes in the bend.

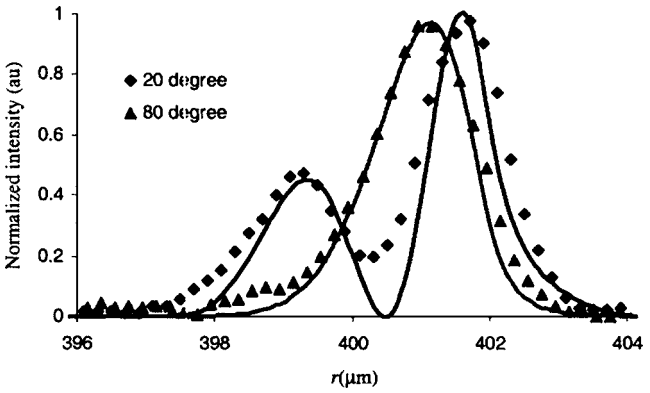

FIG. 5. Optical intensity distributions at different positions. Points are NSOM experimental data and solid curves are the theoretical fit.

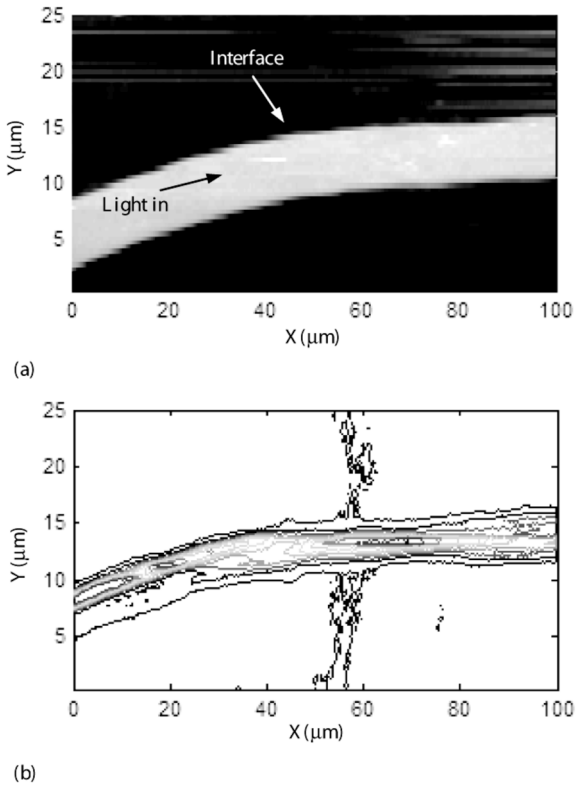

FIG. 6. (a) False intensity image of waveguide topology around the bend-to-straight waveguide interface. (b) Contour plot of optical intensity in the same area.

Additional insertion loss due to scatter is found at the exit interface from the bending waveguide to the straight waveguide. Figure 6(a) shows a NSOM intensity scan of this region. At the end of the bend, 92% of the power is in the fundamental mode, which is strongly shifted toward the outer boundary. However, in the straight waveguide, the power distribution is symmetrically centered for all modes. Therefore, at the interface, scattered light as well as guided modes of the straight waveguide are excited, as clearly seen in Fig. 6(b). The scattering field is observed to be directed perpendicular to the straight waveguide. Further study is needed to understand this observation. However, it is evident that it may be useful to engineer the exit waveguide to match the modes of the bend or otherwise gradually shift the mode toward the center of the straight waveguide to reduce this insertion loss.

In summary, near-field scanning optical microscopy was employed to directly image the modes in a waveguide bend. Interference between the two lowest order modes was observed and fit to obtain the relative amplitude, phase, and attenuation coefficients of the two modes. Conformal mapping of the index profile predicts the modal profiles accurately. Insertion loss due to scattering at the interfaces of the bend and straight waveguides was found and attributed to the modal mismatch.

The authors would like to thank NIH for sponsorship via Grant No. EB00726, Dr. Van Orden for access to NSOM, and Thermo-Electron, Inc. for SiN_x film deposition.

[1]A. Nesterov and U. Troppenz, J. Lightwave Technol. **21**, 2434 (2003).
[2]W. Berglund and A. Gopinath, J. Lightwave Technol. **18**, 1161 (2000).
[3]G. H. Vander Rhodes, B. B. Goldberg, M. S. Ünlü, S. T. Chu, W. Pan, T. Kaneko, Y. Kokobun, and B. E. Little, Appl. Phys. Lett. **75**, 2368 (1999).
[4]S. Bourzeix, J. M. Moison, F. Mignard, F. Barthe, A. C. Borccara, C. Licoppe, B. Mersali, M. Allovon, and A. Bruno, Appl. Phys. Lett. **73**, 1035 (1998).
[5]W. Ji, D. Kim, H. J. Kim, O. Beom-Hoan, S. Park, E. Lee, and S. G. Lee, IEEE Photonics Technol. Lett. **17**, 846 (2005).
[6]A. L. Campillo, J. W. P. Hsu, K. R. Parameswaran, and M. M. Fejer, Opt. Lett. **28**, 399 (2003).
[7]G. W. Yuan, M. D. Stephens, D. S. Dandy, and K. L. Lear, IEEE Photonics Technology Letters (in press).
[8]G. H. Vander Rhodes, B. B. Goldberg, M. S. Unlu, S.-T. Chu, and B. E. Little, IEEE J. Sel. Top. Quantum Electron. **6**, 46 (2000).
[9]N. F. Van Hulst, M. H. P. Moers, O. F. J. Noordman, R. G. Tack, and F. B. Segerink, Appl. Phys. Lett. **62**, 461 (1993).